

DiffWire: Inductive Graph Rewiring via the Lovász Bound

Adrián Arnaiz-Rodríguez
ELLIS Alicante, Spain

adrian@ellisalicante.org

Ahmed Begga
University of Alicante, Spain

Francisco Escolano
ELLIS Alicante, Spain
University of Alicante, Spain

sco@ellisalicante.org

Nuria Oliver
ELLIS Alicante, Spain

nuria@ellisalicante.org

Abstract

Graph Neural Networks (GNNs) have been shown to achieve competitive results to tackle graph-related tasks, such as node and graph classification, link prediction and node and graph clustering in a variety of domains. Most GNNs use a message passing framework and hence are called MPNNs. Despite their promising results, MPNNs have been reported to suffer from over-smoothing, over-squashing and under-reaching. Graph rewiring and graph pooling have been proposed in the literature as solutions to address these limitations. However, most state-of-the-art graph rewiring methods fail to preserve the global topology of the graph, are not differentiable (inductive) and require the tuning of hyper-parameters. In this paper, we propose DIFFWIRE, a novel framework for graph rewiring in MPNNs that is principled, fully differentiable and parameter-free by leveraging the Lovász bound. Our approach provides a unified theory for graph rewiring by proposing two new, complementary layers in MPNNs: first, CT-LAYER, a layer that learns the commute times and uses them as a relevance function for edge re-weighting; second, GAP-LAYER, a layer to optimize the spectral gap, depending on the nature of the network and the task at hand. We empirically validate the value of our proposed approach and each of these layers separately with benchmark datasets for graph classification. DIFFWIRE brings together the learnability of commute times to related definitions of curvature, opening the door to the development of more expressive MPNNs.

1 Introduction

Graph Neural Networks (GNNs) [1, 2] are a class of deep learning models applied to graph structured data. They have been shown to achieve state-of-the-art results in many graph-related tasks, such as node and graph classification [3, 4], link prediction [5] and node and graph clustering [6, 7], and in a variety of domains, including image or molecular structure classification, recommender systems and social influence prediction [8].

Most GNNs use a message passing framework and thus are referred to as Message Passing Neural Networks (MPNNs) [4]. In these networks, every node in each layer receives a message from its adjacent neighbors. All the incoming messages at each node are then aggregated and used to update the node's representation via a learnable non-linear function –which is typically implemented by means of a neural network. The final node representations (called node embeddings) are used to perform the graph-related task at hand (e.g. graph classification). MPNNs are extensible, simple and have proven to yield competitive empirical results. Examples of MPNNs include GCN [3], GAT [9], GATv2 [10], GIN [11] and GraphSAGE [12].

However, MPNNs have important limitations due to the inherent complexity of graphs, the limited depth of most state-of-the-art MPNNs and the inability of current methods to capture global structural information

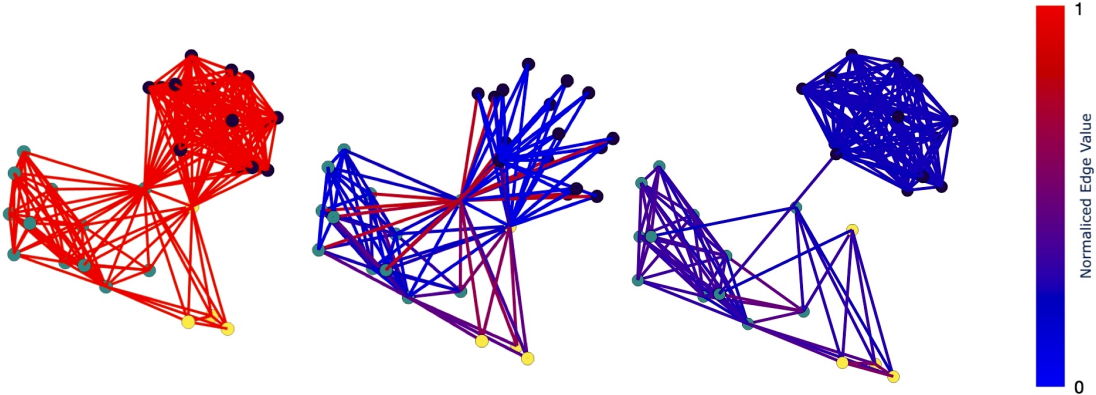


Figure 1: DiffWire. Left: Original graph. Center: Rewired graph after CT-LAYER. Right: Rewired graph after GAP-LAYER. Colors indicate the strength of the edges.

of the graph. The literature has reported best results when MPNNs have a small number of layers, because networks with many layers tend to suffer from *over-smoothing* [13] and *over-squashing* [14]. Over-smoothing takes place when the embeddings of nodes that belong to different classes become indistinguishable. Over-squashing refers to the distortion of information flowing from distant nodes due to graph bottlenecks¹ that emerge when the number of k-hop neighbors grows exponentially with k. They both tend to occur in networks with a large number of layers [15].

Moreover, simple MPNNs with a small number of layers fail to capture information that depends on the entire structure of the graph (e.g., random walk probabilities [16]) and prevent the information flow to reach distant nodes. This phenomenon is called *under-reaching* [17] and occurs when the MPNNs depth is smaller than the graph’s diameter.

Graph pooling and *graph rewiring* have been proposed in the literature as solutions to address these limitations [14]. Given that the main infrastructure for message passing in MPNNs are the edges in the graph, and given that many of these edges might be noisy or inadequate for the downstream task [18], graph rewiring aims to identify such edges and edit them.

Many graph rewiring methods rely on edge sampling strategies: first, the edges are assigned new weights according to a *relevance function* and then they are re-sampled according to the new weights to retain the most relevant edges (i.e. those with larger weights). Edge relevance might be computed in different ways, including randomly [19], based on similarity [20] or the edge curvature [21].

Due to the diversity of possible graphs and tasks to be performed with those graphs, optimal graph rewiring should include a *variety of strategies* that are suited not only to the task at hand but also to the nature and structure of the graph.

State-of-the-art sampling strategies have three significant limitations. First, most of the proposed methods fail to preserve the global topology of the graph. Second, most graph rewiring methods are not differentiable and hence are not inductive [21]. Third, relevance functions that depend on a diffusion measure (typically in the spectral domain) are not parameter-free, which adds a layer of complexity in the models. In this paper, we address these three limitations.

Contributions and outline. The main contribution of our work is to propose a theoretical framework called DIFFWIRE for graph rewiring in MPNNs that is *principled, fully differentiable (inductive) and parameter-free* by leveraging the Lovász bound [16] given by Eq. 1. This bound is a mathematical expression of the relationship between the commute times (effective resistance distance) and the network’s spectral gap. Given the recently reported connection between commute times and curvature [22], and between curvature and the spectral gap [21], our framework provides a unified theory linking these concepts.

¹A graph bottleneck is defined as a topological property of the graph that leads to over-squashing.

We first propose using the commute times as a relevance function for edge re-weighting. Moreover, we develop a differentiable, parameter-free layer in the GNN (CT-LAYER) to learn the commute times. Second, we present a novel graph rewiring approach by adding a layer in the network (GAP-LAYER) that optimizes the spectral gap according to the nature of the network and the task at hand. Finally, we empirically validate the proposed layers with state-of-the-art benchmark datasets in a graph classification task.

The paper is organized as follows: Section 2 provides a summary of the most relevant related literature. Our core technical contribution is described in Section 3, followed by our experimental evaluation and discussion in Section 4. Finally, Section 5 is devoted to conclusions and an outline of our future lines of research.

2 Related Work

In this section we provide an overview of the most relevant works that have been proposed in the literature to tackle the challenges of over-smoothing, over-squashing and under-reaching in MPNNs.

Limitations of MPNNs.

MPNNs are widely used to tackle many real-world tasks –from social network analysis to protein modeling– with competitive results. However, MPNNs also have important limitations due to the inherent complexity of graphs. Despite such complexity, the literature has reported best results when MPNNs have a small number of layers, because networks with many layers tend to suffer from *over-smoothing* [13] and *over-squashing* [14].

Over-smoothing [23, 24, 8, 15] takes place when the embeddings of nodes that belong to different classes become indistinguishable. It tends to occur in MPNNs with many layers that are used to tackle short-range tasks, i.e. tasks where a node’s correct prediction mostly depends on its local neighborhood. Given this local dependency, it makes intuitive sense that adding layers to the network would not help the network’s performance.

Conversely, long-range tasks require as many layers in the network as the range of the interaction between the nodes. However, as the number of layers in the network increases, the number of nodes feeding into each of the node’s receptive field also increases exponentially, leading to *over-squashing* [14, 21]: the information flowing from the receptive field composed of many nodes is compressed in fixed-length node vectors, and hence the graph fails to correctly propagate the messages coming from distant nodes. Thus, over-squashing emerges when there is a *bottleneck* in the graph and a long-range task.

To prevent over-smoothing and over-squashing, the number of layers in MPNNs is typically kept small. However, simple models with a small number of layers fail to capture information that depends on the entire structure of the graph (e.g., random walk probabilities [16]) and prevent the information flow to reach distant nodes. This phenomenon is called *under-reaching* [17] and occurs when the MPNNs depth is smaller than the graph’s diameter.

Graph rewiring in MPNNs. *Rewiring* is a process of changing the graph structure to control the information flow and hence improve the ability of the network to perform the task at hand (e.g. node or graph classification, link prediction...). Several approaches have been proposed in the literature for graph rewiring, such as connectivity diffusion [25] or evolution [21], adding new bridge-nodes [26] and multi-hop filters [27], and neighborhood [12], node [28] or edge [29] sampling.

Edge sampling methods sample the graph’s edges based on their weights or relevance, which might be computed in different ways. Huang et al. prove in [19] that randomly dropping edges during training improves the performance of GNNs. In [25], Klicpera et al. define edge relevance according to the coefficients of a parameterized diffusion process over the graph. Then, the k-hop diffusion matrix is truncated to discard long-range interactions. For Kazi et al. [20], edge relevance is given by the similarity between the nodes’ attributes $p_{ij} = e^{-t\|\hat{x}_i - \hat{x}_j\|^2}$ using a temperature parameter t . In addition, a reinforcement learning process rewards edges leading to a correct classification and penalizes the rest.

Edge sampling-based rewiring has been proposed to tackle over-smoothing and over-squashing in MPNNs. Over-smoothing may be relieved by removing inter-class edges [30]. However, this strategy is only valid when

the graph is homophilic². Otherwise, removing these edges could lead to over-squashing [21] if their removal obstructs the message passing between distant nodes belonging to the same class (heterophily). Increasing the size of the bottlenecks of the graph via rewiring has been shown to improve node classification performance in heterophilic graphs, but not in homophilic graphs [21]. Recently, Topping et al. [21] propose an edge relevance function given by the edge curvature to mitigate over-squashing. They identify the bottleneck of the graph by computing the Ricci curvature of the edges. Next, they remove edges with high curvature and add edges around minimal curvature edges.

Pooling in MPNNs. In addition to graph rewiring, most MPNNs include *pooling* layers to simplify the original graph by compressing it into a smaller graph or a vector via pooling operators, which range from simple (e.g. mean, sum or max operators applied to all node representations) [31] to more sophisticated approaches, such as

DiffPool [32] and MinCut pool [33]. Alternative approaches [34, 35] address the problem as a top-K pooling method, and prune nodes based on a projection score using a learnable function of the node features. Several authors propose selecting relevant clusters [36] or using attention-based operations to model the relationships between clusters [37]. Note that graph pooling methods do not consider the edge representations and hence are complementary to edge re-wiring approaches. However, there is a clear relationship between pooling methods and rewiring since both of them try to reduce the flow of information through the graph’s bottleneck.

3 Proposed Approach: DiffWire for Inductive Graph Rewiring

3.1 The Lovász Bound and beyond

The Lovász Bound. The Lovász bound, given by Eq. 1, was derived in Lovász [16] as a means of linking the spectrum governing a random walk in an undirected graph $G = (V, E)$ with the *hitting time* H_{uv} between any two nodes u and v of the graph. H_{uv} is the expected number of steps needed to reach (or hit) v from u ; H_{vu} is defined similarly. The sum of both hitting times between the two nodes, v and u , is the *commute time* $CT_{uv} = H_{uv} + H_{vu}$. Thus, CT_{uv} is the expected number of steps needed to hit v from u and then going back to u .

$$\left| \frac{1}{\text{vol}(G)} CT_{uv} - \left(\frac{1}{d_u} + \frac{1}{d_v} \right) \right| \leq \frac{1}{\lambda'_2} \frac{2}{d_{\min}} \quad (1)$$

In the bound above, $\lambda'_2 \geq 0$ is the *spectral gap*, i.e. the first non-zero eigenvalue of $\mathcal{L} = \mathbf{I} - \mathbf{D}^{-1/2} \mathbf{A} \mathbf{D}^{-1/2}$ (normalized Laplacian [38], where \mathbf{D} is the degree matrix of the graph and \mathbf{A} , the adjacency matrix); $\text{vol}(G)$ is the volume of the graph (sum of degrees); d_u and d_v are the degrees of nodes u and v , respectively; and d_{\min} is the minimum degree of the graph.

The left term in the subtraction in Eq. 1, i.e. $CT_{uv}/\text{vol}(G)$, is referred to as the *effective resistance*, R_{uv} , between nodes u and v . The bound states that the effective resistance between two nodes in the graph converges to or diverges from $(1/d_u + 1/d_v)$, depending on whether the graph’s spectral gap diverges from or tends to zero.

The von Luxburg et al. Bound. The Lovász bound was later refined by von Luxburg et al. [39] via a new, tighter bound which replaces d_{\min} by d_{\min}^2 in Eq. 1. Given that $\lambda'_2 \in (0, 2]$, when the number of nodes in the graph ($n = |V|$) and the average degree increase, then $R_{uv} \approx 1/d_u + 1/d_v$. This is likely to happen in certain types of graphs, such as Gaussian similarity-graphs –graphs where two nodes are linked if the neg-exponential of the distances between the respective features of the nodes is strong enough; ϵ -graphs –graphs where the Euclidean distances between the features in the nodes are less or equal than ϵ ; and k –NN graphs with large k wrt n . The authors report a linear collapse of R_{uv} with the density of the graph in scale-free networks, such as social network graphs, whereas a fast collapse of R_{uv} has been reported in community graphs –congruent graphs with Stochastic Block Models (SBMs) [40].

²A homophilic graph is a graph where connected nodes tend to share similar attributes.

Given the importance of the effective resistance, R_{uv} , as a *global* measure of node similarity, the von Luxburg et al.'s refinement motivated the development of *robust effective resistances*, mostly in the form of p -resistances given by $R_{uv}^p = \arg \min_{\mathbf{f}} \{\sum_{e \in E} r_e |f_e|^p\}$, where \mathbf{f} is a unit-flow injected in u and recovered in v ; and $r_e = 1/w_e$ with w_e being the edge's weight [41]. For $p = 1$, R_{uv}^p corresponds to the shortest path; $p = 2$ results in the effective resistance; and $p \rightarrow \infty$ leads to the inverse of the unweighted u - v -mincut³. Therefore, the optimal p value depends on the type of graph [41]. Note that p -resistances can be studied from the perspective of p -Laplacians [42, 43].

Alternatively, R_{uv} could be unbound by minimizing the spectral gap λ_2' . However, this approach has been bypassed by the mathematical characterization of graphs with small spectral gaps [44][45].

Once we have defined both sides of the Lovász and von Luxburg bounds, we proceed to describe their respective implications for graph rewiring.

3.2 CT-Layer: Commute Times for Graph Rewiring

Spectral Sparsification leads to Commute Times. Graph sparsification in undirected graphs has been formulated in terms of finding a graph $H = (V, E')$ that is *spectrally similar* to the original graph $G = (V, E)$ with $E' \subset E$. Hence, the spectra of their respective Laplacians, \mathbf{L}_G and \mathbf{L}_H are similar.

Theorem 1 (Spielman and Srivastava [46]). *Let $G' = \text{Sparsify}(G, q)$ be a sampling algorithm of graph $G = (V, E)$, where edges $e \in E$ are sampled with probability $q \propto R_e$ (proportional to the effective resistance). Then, for $n = |V|$ sufficiently large and $1/\sqrt{n} < \epsilon \leq 1$, we need $O(n \log n / \epsilon^2)$ samples to satisfy*

$$\forall \mathbf{x} \in \mathbb{R}^n : (1 - \epsilon) \mathbf{x}^T \mathbf{L}_G \mathbf{x} \leq \mathbf{x}^T \mathbf{L}_{G'} \mathbf{x} \leq (1 + \epsilon) \mathbf{x}^T \mathbf{L}_G \mathbf{x}, \quad (2)$$

with probability at least 1/2.

The above theorem has a simple explanation in terms of Dirichlet energies. The Laplacian $\mathbf{L} = \mathbf{D} - \mathbf{A} \succcurlyeq 0$, i.e. it is semi-definite positive (all its eigenvalues are non-negative). Then, if we consider $\mathbf{x} : V \rightarrow \mathbb{R}$ as a real-valued function of the n nodes of $G = (V, E)$, we have that $\mathcal{E}(\mathbf{x}) := \mathbf{x}^T \mathbf{L} \mathbf{x} = \sum_{e=(u,v) \in E} (\mathbf{x}_u - \mathbf{x}_v)^2 \geq 0$ for any \mathbf{x} . In particular, the eigenvectors $\mathbf{f} := \{\mathbf{x}_i : \mathbf{L}\mathbf{f}_i = \lambda_i \mathbf{x}_i\}$ are the set of special functions (mutually orthogonal and normalized) that minimize the energies $\mathcal{E}(\mathbf{f}_i)$, i.e. they are the orthogonal functions with the minimal variabilities achievable by the topology of G . Therefore, Theorem 1 states that any minimal variability of G' is bounded by $(1 \pm \epsilon)$ times that of G if we sample enough edges with probability $q \propto R_e$. Therefore, the effective resistance is a *principled relevance function*, since the resulting graph G' retains the main properties of G . In particular, we have that the spectra of \mathbf{L}_G and $\mathbf{L}_{G'}$ are related by $(1 - \epsilon)\lambda_i^G \leq \lambda_i^{G'} \leq (1 + \epsilon)\lambda_i^G$: in short $(1 - \epsilon)\mathbf{L}_G \preccurlyeq \mathbf{L}_{G'} \preccurlyeq (1 + \epsilon)\mathbf{L}_G$. This is a direct result of the theorem since $\lambda_i = \frac{\mathcal{E}(\mathbf{f}_i)}{\mathbf{f}_i^T \mathbf{f}_i}$ are the normalized minimal variabilities.

Commute Times Embedding. The choice of effective resistances⁴ in Theorem 1 is explained by the fact that R_{uv} can be computed from $R_{uv} = (\mathbf{e}_u - \mathbf{e}_v)^T \mathbf{L}^+ (\mathbf{e}_u - \mathbf{e}_v)$, where \mathbf{e}_u is the unit vector with a unit value at u and zero elsewhere. $\mathbf{L}^+ = \sum_{i \geq 2} \lambda_i^{-1} \mathbf{f}_i \mathbf{f}_i^T$, where \mathbf{f}_i, λ_i are the eigenvectors and eigenvalues of \mathbf{L} , is the pseudo-inverse or Green's function of $G = (V, E)$ if it is connected, and from the theorem we also have $(1 + \epsilon)^{-1} \mathbf{L}_G^+ \preccurlyeq \mathbf{L}_{G'}^+ \preccurlyeq (1 - \epsilon)^{-1} \mathbf{L}_G^+$.

The Green's function leads to envision R_{uv} (and therefore CT_{uv}) as *metrics* relating pairs of nodes of G . For instance $\mathbf{R}_{uv} = \mathbf{L}_{uu}^+ + \mathbf{L}_{vv}^+ - 2\mathbf{L}_{uv}^+$, is the resistance distance [47] i.e., as noted by Qiu and Hancock [48] the elements \mathbf{L}_{uv}^+ encode dot products between the *embeddings* \mathbf{z}_u and \mathbf{z}_v of u and v . As a result, the latent space can not only be described spectrally but also in a *parameter free*-manner, which is not the case for other spectral embeddings, such as heat kernel or diffusion maps as they rely on a time parameter t . More precisely, the embedding matrix \mathbf{Z} whose columns contain the nodes embeddings is given by:

$$\mathbf{Z} := \sqrt{\text{vol}(G)} \Lambda'^{-1/2} \mathbf{F}^T = \sqrt{\text{vol}(G)} \Lambda'^{-1/2} \mathbf{G}^T \mathbf{D}^{-1/2} \quad (3)$$

³The link between CTs and mincuts is leveraged later in the paper as an essential element of our approach.

⁴We use CTs and Rs interchangeably as per their use in the literature

where Λ is the diagonal matrix of the unnormalized Laplacian \mathbf{L} eigenvalues and \mathbf{F} is the matrix of their associated eigenvectors. Similarly, Λ' contains the eigenvalues of the normalized Laplacian \mathcal{L} and \mathbf{G} the eigenvectors. We have $\mathbf{F} = \mathbf{G}\mathbf{D}^{-1/2}$ or $\mathbf{f}_i = \mathbf{g}_i\mathbf{D}^{-1/2}$, where \mathbf{D} is the degree matrix.

Finally, the commute times/resistance distances are given by the Euclidean distances between the embeddings $CT_{uv} = \|\mathbf{z}_u - \mathbf{z}_v\|^2$. Their spectral form is

$$R_{uv} = \frac{CT_{uv}}{\text{vol}(G)} = \sum_{i=2}^n \frac{1}{\lambda_i} (\mathbf{f}_i(u) - \mathbf{f}_i(v))^2 = \sum_{i=2}^n \frac{1}{\lambda'_i} \left(\frac{\mathbf{g}_i(u)}{\sqrt{d_u}} - \frac{\mathbf{g}_i(v)}{\sqrt{d_v}} \right)^2 \quad (4)$$

The above spectral expansions evidence that commute times (or resistance distances) rely on the *Fiedler vector* \mathbf{f}_2 (or \mathbf{g}_2) downsampled by the *spectral gap* λ_2 (or more formally λ'_2). The downsampled Fiedler vector dominates the expansion because the Fiedler vector is the solution to the relaxed ratio-cut problem. This is consistent with the fact that p -resistances become the inverse of mincut when $p \rightarrow \infty$.

Commute Times as an Optimization Problem. Constraining neighboring nodes to have a similar embedding leads to

$$\mathbf{Z} = \arg \min_{\mathbf{Z}^T \mathbf{Z} = \mathbf{I}} \frac{\sum_{u,v} \|\mathbf{z}_u - \mathbf{z}_v\|^2 \mathbf{A}_{uv}}{\sum_{u,v} \mathbf{Z}_{uv}^2 d_u} = \frac{\sum_{(u,v) \in E} \|\mathbf{z}_u - \mathbf{z}_v\|^2}{\sum_{u,v} \mathbf{Z}_{uv}^2 d_u} = \frac{\text{Tr}[\mathbf{Z}^T \mathbf{L} \mathbf{Z}]}{\text{Tr}[\mathbf{Z}^T \mathbf{D} \mathbf{Z}]}, \quad (5)$$

which reveals that CTs embeddings result from a Laplacian regularization down-weighted by the degree. As a result, hubs will be embedded far away from their neighbors: *bordeline* nodes –i.e. nodes with inter-cluster edges– tend to have larger degrees than those lying inside their respective communities and the CTs embedding tends to push them away, increasing the *distance* between communities. In addition, note that the above *quotient of traces* formulation is easily differentiable and different from the *traces of quotient* $\text{Tr}[\frac{\mathbf{Z}^T \mathbf{L} \mathbf{Z}}{\mathbf{Z}^T \mathbf{D} \mathbf{Z}}]$ formulation proposed in [48].

With the above elements we have a definition of, CT-LAYER, our first rewiring layer:

Definition 1 (CT-Layer). *Given the matrix $\mathbf{X}_{n \times F}$ encoding the features of the nodes after any message passing (MP) layer, $\mathbf{Z}_{n \times O(n)} = \tanh(\text{MLP}(\mathbf{X}))$ learns the association $\mathbf{X} \rightarrow \mathbf{Z}$ while \mathbf{Z} is optimized according to the loss $L_{CT} = \frac{\text{Tr}[\mathbf{Z}^T \mathbf{L} \mathbf{Z}]}{\text{Tr}[\mathbf{Z}^T \mathbf{D} \mathbf{Z}]} + \left\| \frac{\mathbf{Z}^T \mathbf{Z}}{\|\mathbf{Z}^T \mathbf{Z}\|_F} - \mathbf{I}_n \right\|_F$. This results in the following resistance diffusion $\mathbf{T}^{CT} = \mathbf{R}(\mathbf{S}) \odot \mathbf{A}$ (Hadamard product between the resistance distance and the adjacency) which provides as input to the subsequent MP layer a learnt convolution matrix.*

\mathbf{T}^{CT} and Graph Bottlenecks. Beyond the principled sparsification of \mathbf{T}^{CT} (enabled by Theorem 1), this matrix rewrites the graph $G = (E, V)$ in a way that edges with maximal resistance tend to be the most critical to preserve the topology of the graph. More precisely, although $\sum_{e \in E} R_e = n - 1$, the bulk of the resistance distribution is located at graph bottlenecks, if they exist. Otherwise, their magnitude is upper-bounded and the distribution becomes more uniform.

Graph bottlenecks are controlled by the *graph conductance* (Cheeger constant) $h_G = \min_{S \subseteq V} h_S$, where: $h_S = \frac{|\partial S|}{\min(\text{vol}(S), \text{vol}(\bar{S}))}$, $\partial S = \{e = (u, v) : u \in S, v \in \bar{S}\}$ and $\text{vol}(S) = \sum_{u \in S} d_u$. The following theorem captures the interplay between graph conductance and effective resistances:

Theorem 2 (Alev et al. [49]). *Given a graph $G = (V, E)$, a subset $S \subseteq V$ with $\text{vol}(S) \leq \text{vol}(G)/2$, we have*

$$h_S \geq \frac{c}{\text{vol}(S)^{1/2-\epsilon}} \iff |\partial S| \geq c \cdot \text{vol}(S)^{1/2-\epsilon}, \quad (6)$$

for some constant c and $\epsilon \in [0, 1/2]$. Then, for any pair u, v we have $R_{uv} \leq \left(\frac{1}{d_u^{2\epsilon}} + \frac{1}{d_v^{2\epsilon}} \right) \cdot \frac{1}{\epsilon \cdot c^2}$.

This theorem shows that the larger the bottleneck the more bounded the resistance distances are. In addition, from this theorem we have $\max(R_{uv}) \leq 1/h_S^2$, i.e., the resistance is bounded by the square of the bottleneck. This bound partially explains the rewiring of the graph in Figure 1-center. As seen in the Figure, rewiring using the CTs sparsifies the graph and assigns larger weights to the edges in the graph's bottleneck whereas non-essential edges are given low weights. We explore the interplay between the above theorem and Theorem 1 in Appendix A.

Effective Resistances and Curvature. In [21], Topping et al. propose an interesting approach for graph rewiring, where the relevance function is given by the Ricci curvature. However, this measure is non-differentiable. More recent definitions of curvature [22] have been formulated based on resistance distances, and the would be differentiable with our approach. The resistance curvature of an edge $e = (u, v)$ is $\kappa_{uv} := 2(p_u + p_v)/R_{uv}$ where $p_u := 1 - \frac{1}{2} \sum_{w \sim u} R_{uw}$ is the node curvature. The following theorem summarizes several, relevant properties that will be discussed in Appendix A.

Theorem 3 (Devriendt and Lambiotte [22]). *The edge resistance curvature has the following properties: (1) It is bounded by $(4 - d_u - d_v) \leq \kappa_{uv} \leq 2/R_{uv}$, with equality in the lower bound iff all incident edges to u and v are cut links; (2) It is upper-bounded by the Ollivier-Ricci curvature $\kappa_{uv}^{OR} \geq \kappa_{uv}$, with equality if (u, v) is a cut link; and (3) Forman-Ricci curvature: $\kappa_{uv}^{FR}/R_{uv} \leq \kappa_{uv}$ with equality at cut links.*

3.3 GAP-Layer: Spectral Gap Optimization for Graph Rewiring

The right-hand side of the Lovász bound relies on the spectral gap λ'_2 in such a way that the larger the spectral gap, the closer the commute times would be to their non-informative regime. In addition, the spectral graph is typically large in commonly observed graphs –such as communities in social networks which may be bridged by many edges [40]– and, hence, it is desirable to rewire the adjacency matrix \mathbf{A} so that λ'_2 is minimized.

Ratio-cut (Rcut) Approximation. In a first approximation, we rewire the adjacency matrix, \mathbf{A} , so that λ_2 is minimized. We consider a matrix $\tilde{\mathbf{A}}$ close to \mathbf{A} that satisfies $\tilde{\mathbf{L}}\mathbf{f}_2 = \lambda_2\mathbf{f}_2$, where \mathbf{f}_2 is the solution to the ratio-cut relaxation [42]. Following [50], the gradient of λ_2 wrt each component of $\tilde{\mathbf{A}}$ is given by

$$\nabla_{\tilde{\mathbf{A}}}\lambda_2 := Tr \left[(\nabla_{\tilde{\mathbf{L}}}\lambda_2)^T \cdot \nabla_{\tilde{\mathbf{A}}}\tilde{\mathbf{L}} \right] = \text{diag}(\mathbf{f}_2\mathbf{f}_2^T)\mathbf{1}\mathbf{1}^T - \mathbf{f}_2\mathbf{f}_2^T, \quad (7)$$

where $\mathbf{1}$ is the vector of n ones; and $[\nabla_{\tilde{\mathbf{A}}}\lambda_2]_{ij}$ is the gradient of λ_2 wrt $\tilde{\mathbf{A}}_{uv}$. The driving force of this gradient relies on the correlation $\mathbf{f}_2\mathbf{f}_2^T$. As explained in Appendix B, using this gradient to minimize λ_2 results in breaking the bottleneck while preserving simultaneously the inter-cluster structure.

Normalized-cut (Ncut) Approximation. Similarly, considering now λ'_2 for rewiring leads to

$$\begin{aligned} \nabla_{\tilde{\mathbf{A}}}\lambda'_2 &:= Tr \left[(\nabla_{\tilde{\mathcal{L}}}\lambda_2)^T \cdot \nabla_{\tilde{\mathbf{A}}}\tilde{\mathcal{L}} \right] = \\ \mathbf{d}' \left\{ \mathbf{g}_2^T \tilde{\mathbf{A}}^T \tilde{\mathbf{D}}^{-1/2} \mathbf{g}_2 \right\} \mathbf{1}^T + \mathbf{d}' \left\{ \mathbf{g}_2^T \tilde{\mathbf{A}} \tilde{\mathbf{D}}^{-1/2} \mathbf{g}_2 \right\} \mathbf{1}^T &+ \tilde{\mathbf{D}}^{-1/2} \mathbf{g}_2 \mathbf{g}_2^T \tilde{\mathbf{D}}^{-1/2} \end{aligned} \quad (8)$$

where \mathbf{d}' is a $n \times 1$ vector including derivatives of degree wrt adjacency and related terms. This gradient relies on the Fiedler vector \mathbf{g}_2 (now the solution to the normalized-cut relaxation), but also on the incoming and outgoing one-hop random walks. This approximation breaks the bottleneck while preserving the global topology of the graph (Figure 1-left). More details and proof are included in Appendix B.

Approximating the Fiedler vector. Given that $\mathbf{g}_2 = \tilde{\mathbf{D}}^{1/2}\mathbf{f}_2$, we can obtain the normalized-cut gradient in terms of \mathbf{f}_2 . From [23] we have that

$$\mathbf{f}_2(u) = \begin{cases} +1/\sqrt{n} & \text{if } u \text{ belongs to the first cluster} \\ -1/\sqrt{n} & \text{if } u \text{ belongs to the second cluster} \end{cases} + O\left(\frac{\log n}{n}\right) \quad (9)$$

Definition 2 (GAP-Layer). *Given the matrix $\mathbf{X}_{n \times F}$ encoding the features of the nodes after any message passing (MP) layer, $\mathbf{S}_{n \times 2} = \text{Softmax}(MLP(\mathbf{X}))$ learns the association $\mathbf{X} \rightarrow \mathbf{S}$ while \mathbf{S} is optimized according to the loss $L_{Cut} = -\frac{Tr[\mathbf{S}^T \mathbf{AS}]}{Tr[\mathbf{S}^T \mathbf{DS}]} + \left\| \frac{\mathbf{S}^T \mathbf{S}}{\|\mathbf{S}^T \mathbf{S}\|_F} - \frac{\mathbf{I}_n}{\sqrt{2}} \right\|_F$. Then the Fiedler vector \mathbf{f}_2 is approximated by applying a softmaxed version of Eq. 9 and we consider the loss $L_{Fiedler} = \|\tilde{\mathbf{A}} - \mathbf{A}\|_F + \alpha(\lambda_2^*)^2$ where $\lambda_2^* = \lambda_2$ if we use the ratio-cut approximation (and gradient) and $\lambda_2^* = \lambda'_2$ if we use the normalized-cut approximation and gradient. This returns $\tilde{\mathbf{A}}$. Then the GAP diffusion $\mathbf{T}^{GAP} = \tilde{\mathbf{A}}(\mathbf{S}) \odot \mathbf{A}$ results from minimizing $L_{GAP} := L_{Cut} + L_{Fiedler}$.*

Table 1: Experimental results on common graph classification benchmarks. **Red** denotes the best model for the dataset and **blue** marks the runner-up. Degree is used as the node features in datasets marked with *.

	MinCutPool	DIGL	CT-LAYER	GAP-LAYER (Rcut)	GAP-LAYER (Ncut)
REDDIT-BINARY*	66.53 ± 4.47	76.02 ± 4.31	78.45 ± 4.59	77.63 ± 4.96	76.00 ± 5.30
IMDB-BINARY*	60.75 ± 7.03	59.35 ± 7.76	69.84 ± 4.60	69.93 ± 3.32	68.80 ± 3.10
COLLAB*	58.00 ± 6.22	57.51 ± 5.95	69.87 ± 2.40	64.47 ± 4.07	65.89 ± 4.90
MUTAG	84.21 ± 6.34	85.00 ± 5.65	86.05 ± 4.99	86.90 ± 4.00	86.90 ± 4.00
PROTEINS	74.84 ± 2.39	74.49 ± 2.88	75.38 ± 2.97	75.03 ± 3.09	75.34 ± 2.10
SBM*	53.00 ± 9.90	56.93 ± 12.8	81.40 ± 11.7	90.80 ± 7.00	92.26 ± 2.92
Erdös-Rényi*	81.86 ± 6.26	81.93 ± 6.32	79.06 ± 9.89	79.26 ± 10.46	82.26 ± 3.20

4 Experiments and Discussion

Experimental setup. To validate our approach, we carry out several experiments on benchmark datasets for graph classification and compare the proposed rewiring layers (CT-LAYER and GAP-LAYER) with 2 state-of-the-art baselines (MinCut Pool and DIGL). Our goal is to measure and analyze empirically the impact of adding separately each of our proposed layers in a graph classification task. We compare our approach with the two baseline architectures described next.

Baseline1: MinCut Pool. The first baseline architecture is based on MINCUT Pool and it is composed of: Linear(\mathbf{X}) → Conv1(\mathbf{A}, \mathbf{X}) → MINCUTPOOL(\mathbf{A}, \mathbf{X}) → Conv2(\mathbf{A}', \mathbf{X}) → Readout → MLP. MINCUTPOOL learns $(\mathbf{A}_{n \times n}, \mathbf{X}_{n \times F}) \rightarrow (\mathbf{A}'_{k \times k}, \mathbf{X}_{k \times F})$, being k the new number of node clusters.

Baseline2: DIGL. The second baseline architecture is based on DIGL (PPR) with teleporting probability α and ϵ -thresholding parameters [25]. Klicpera et al. [25] perform a hyper-parameter search for each graph. As our task is graph classification, this search is computationally very expensive: $O(n^3)$ per graph. Therefore, we use a fixed $\alpha = 0.001$ and ϵ based on keeping the same average degree for each graph. Once preprocessed using DIGL, the graphs are provided as input to the MinCut Pool (Baseline1) arquitecture.

To evaluate CT-LAYER and GAP-LAYER, we add the corresponding layer in between Linear(\mathbf{X}) → Conv1(\mathbf{A}, \mathbf{X}). We build 3 different models: CT-LAYER, GAP-LAYER (Rcut), GAP-LAYER (Ncut), depending on the layer used. For CT-LAYER, we learn \mathbf{T}^{CT} which is used as a convolution matrix afterwards. For GAP-LAYER, we learn \mathbf{T}^{GAP} either using the Rcut or the Ncut approximations.

As shown in Table 1, we use in our experiments common benchmark datasets for graph classification. We select datasets both with features and featureless, in which case we use the degree as the node features. These datasets are diverse regarding the topology of their networks: REDDIT-BINARY, IMDB-BINARY and COLLAB contain truncate scale-free graphs (social networks), whereas MUTAG and PROTEINS contain graphs from biology or chemistry. In addition, we use two synthetic datasets with 2 classes: Erdös-Rényi with $p_1 \in [0.3, 0.5]$ and $p_2 \in [0.4, 0.8]$ and Stochastic block model (SBM) with parameters $p_1 = 0.8$, $p_2 = 0.5$, $q_1 \in [0.1, 0.15]$ and $q_2 \in [0.01, 0.1]$.

We report average accuracies and standard deviation on 10 random data splits, using 80/20 train-test split, training during 60 epochs and reporting the results of the last epoch for each random run. We use Pytorch Geometric framework for our experiments and our code is publicly available ⁵. Results are shown in Table 1.

Results in graph classification The experiments support our hypothesis that rewiring based on CT-LAYER and GAP-LAYER improves the performance of the baselines, due to its clear relationship with both curvature and classical graph theory. Since both layers are differentiable, our approach allows to learn how to rewire unseen graphs. The improvements are significant in graphs where social components arise (e.g. REDDITB, IMDBB, COLLAB), i.e. graphs with small world properties and power-law degree distributions with a topology based on hubs and authorities. Note that in that class of networks, bottlenecks arise easily and our approach is able to properly rewire the graphs. However, the improvements observed in planar or

⁵<https://anonymous.4open.science/r/DiffWireNeurIPS22/readme.md>

grid networks (e.g. MUTAG AND PROTEINS) are much more limited. These are networks where the bottleneck is not critical for the graph classification task (e.g., chemistry/biology-based networks).

In addition, our method performs better in graphs with no features than in graphs with features because it is able to leverage the information encoded in the topology of the graphs. Note that in attribute-based graphs, the weights of the attributes typically overwrite the graph structure in the classification task, whereas in graphs without features, the information is encoded in the graph’s structure.

Observing the latent space of the REDDIT-BINARY dataset (Figure 2), CT-LAYER creates a disperse yet structured latent space for the embeddings of the graphs, which means that it is able to capture different topological details. GAP-LAYER creates a latent space where, although the 2 classes are also separable, the embeddings are more compressed, due to a more aggressive –yet still informative– change in topology. However, MINCUT creates a more squeezed and compressed embedding, where both classes lie in the same spaces and most of the graphs have collapsed representations.

The real-world datasets explored in this paper are characterized by mild bottlenecks from the perspective of the Lovász bound. For completion, we have included two synthetic datasets (SMB and Erdős-Rényi) where the Lovász bound is very restrictive. As a result, CT-LAYER is outperformed by GAP-LAYER in SMB, and CT-LAYER is also outperformed by DIGL in Erdős-Rényi. Note that the results on the synthetic datasets suffer from large variability.

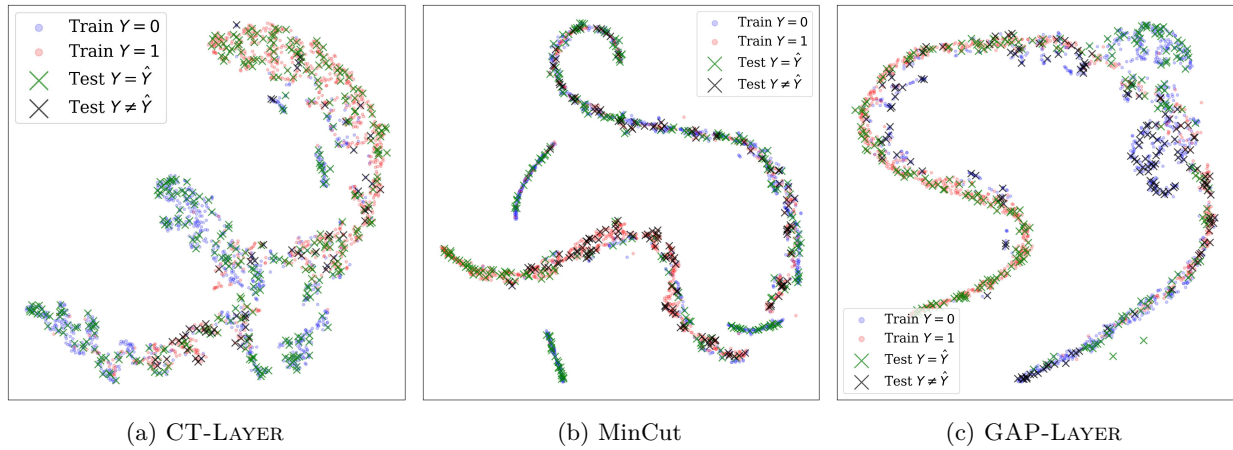


Figure 2: REDDIT embeddings produced by GAP-LAYER (Ncut) CT-LAYER and MINCUT.

5 Conclusion and Future Work

In this paper, we have proposed a unified framework for graph rewiring by linking the two main ingredients of the Lovász bound: CTs distances and the spectral gap. We have developed two novel, fully differentiable (inductive) rewiring layers – CT-LAYER and GAP-LAYER. We have empirically evaluated these layers on benchmark datasets for graph classification and have obtained competitive results when compared to state-of-the-art baselines, specially in graphs where the nodes have no attributes.

In terms of future work, we plan to test our approach in other graph-related tasks, such as node classification, link prediction and graph regression (autoencoders). We also plan to couple CT-LAYER and GAP-LAYER in the same architecture, and explore the expressiveness of the resulting approach. Preliminary findings are included in Appendix C.

Finally, we intend to apply this technique to real-world applications beyond the classical GNN tasks. Specifically, we will delve into the analysis and application of rewiring in social networks, which have unique topology, statistics and, above all, direct implications in society.

Acknowledgements and funding disclosure A. Arnaiz-Rodríguez and N. Oliver are supported by a nominal grant received at the ELLIS Unit Alicante Foundation from the Regional Government of Valencia in Spain (Convenio Singular signed with Generalitat Valenciana, Conselleria d’Innovació, Universitats, Ciència i Societat Digital, Dirección General para el Avance de la Sociedad Digital). A. Arnaiz-Rodríguez is also funded by a grant by the Banc Sabadell Foundation. F. Escolano is funded by the project RTI2018-096223-B-I00 of the Spanish Government.

References

- [1] Marco Gori, Gabriele Monfardini, and Franco Scarselli. A new model for learning in graph domains. In *Proceedings. 2005 IEEE international joint conference on neural networks*, volume 2, pages 729–734, 2005. 1
- [2] Franco Scarselli, Marco Gori, Ah Chung Tsoi, Markus Hagenbuchner, and Gabriele Monfardini. The graph neural network model. *IEEE transactions on neural networks*, 20(1):61–80, 2008. 1
- [3] Thomas N. Kipf and Max Welling. Semi-supervised classification with graph convolutional networks. In *International Conference on Learning Representations (ICLR)*, 2017. 1
- [4] Justin Gilmer, Samuel S. Schoenholz, Patrick F. Riley, Oriol Vinyals, and George E. Dahl. Neural message passing for quantum chemistry. In *Proceedings of the 34th International Conference on Machine Learning - Volume 70*, ICML’17, page 1263–1272. JMLR.org, 2017. 1
- [5] Thomas N Kipf and Max Welling. Variational graph auto-encoders. In NeurIPS Workshop on Bayesian Deep Learning, 2016. 1
- [6] Shaosheng Cao, Wei Lu, and Qiongkai Xu. Deep neural networks for learning graph representations. In *Proceedings of the AAAI Conference on Artificial Intelligence*, volume 30, 2016. 1
- [7] Fei Tian, Bin Gao, Qing Cui, Enhong Chen, and Tie-Yan Liu. Learning deep representations for graph clustering. In *Proceedings of the AAAI Conference on Artificial Intelligence*, volume 28, 2014. 1
- [8] Zonghan Wu, Shirui Pan, Fengwen Chen, Guodong Long, Chengqi Zhang, and Philip S. Yu. A comprehensive survey on graph neural networks. *IEEE Transactions on Neural Networks and Learning Systems*, 32(1):4–24, 2021. 1, 3
- [9] Petar Veličković, Guillem Cucurull, Arantxa Casanova, Adriana Romero, Pietro Liò, and Yoshua Bengio. Graph Attention Networks. *International Conference on Learning Representations*, 2018. 1
- [10] Shaked Brody, Uri Alon, and Eran Yahav. How attentive are graph attention networks? *arXiv preprint arXiv:2105.14491*, 2021. 1
- [11] Keyulu Xu, Weihua Hu, Jure Leskovec, and Stefanie Jegelka. How powerful are graph neural networks? In *International Conference on Learning Representations*, 2019. 1
- [12] William L. Hamilton, Rex Ying, and Jure Leskovec. Inductive representation learning on large graphs. In *Proceedings of the 31rd International Conference on NeurIPS*, 2017. 1, 3
- [13] Qimai Li, Zhichao Han, and Xiao-Ming Wu. Deeper insights into graph convolutional networks for semi-supervised learning. In *Proceedings of the Thirty-Second AAAI Conference on Artificial Intelligence and Thirtieth Innovative Applications of Artificial Intelligence Conference and Eighth AAAI Symposium on Educational Advances in Artificial Intelligence, AAAI’18/IAAI’18/EAAI’18*. AAAI Press, 2018. 2, 3
- [14] Uri Alon and Eran Yahav. On the bottleneck of graph neural networks and its practical implications. In *International Conference on Learning Representations*, 2021. 2, 3
- [15] Jie Zhou, Ganqu Cui, Zhengyan Zhang, Cheng Yang, Zhiyuan Liu, and Maosong Sun. Graph neural networks: A review of methods and applications. *CoRR*, abs/1812.08434, 2018. 2, 3
- [16] L. Lovász. Random walks on graphs: A survey. In D. Miklós, V. T. Sós, and T. Szőnyi, editors, *Combinatorics, Paul Erdős is Eighty*, volume 2, pages 353–398. János Bolyai Mathematical Society, Budapest, 1996. 2, 3, 4
- [17] Pablo Barceló, Egor V. Kostylev, Mikael Monet, Jorge Pérez, Juan Reutter, and Juan Pablo Silva. The logical expressiveness of graph neural networks. In *International Conference on Learning Representations*, 2020. 2, 3

-
- [18] Petar Veličković. Message passing all the way up. In *ICLR 2022 Workshop on Geometrical and Topological Representation Learning*, 2022. 2
- [19] Wenbing Huang, Yu Rong, Tingyang Xu, Fuchun Sun, and Junzhou Huang. Tackling over-smoothing for general graph convolutional networks. *arXiv preprint arXiv:2008.09864*, 2020. 2, 3
- [20] Anees Kazi, Luca Cosmo, Seyed-Ahmad Ahmadi, Nassir Navab, and Michael Bronstein. Differentiable graph module (dgm) for graph convolutional networks. *IEEE Transactions on Pattern Analysis and Machine Intelligence*, pages 1–1, 2022. 2, 3
- [21] Jake Topping, Francesco Di Giovanni, Benjamin Paul Chamberlain, Xiaowen Dong, and Michael M. Bronstein. Understanding over-squashing and bottlenecks on graphs via curvature. In *International Conference on Learning Representations*, 2022. 2, 3, 4, 7, 17
- [22] Karel Devriendt and Renaud Lambiotte. Discrete curvature on graphs from the effective resistance. *arXiv preprint arXiv:2201.06385*, 2022. 2, 7, 17
- [23] NT Hoang, Takanori Maehara, and Tsuyoshi Murata. Revisiting graph neural networks: Graph filtering perspective. In *2020 25th International Conference on Pattern Recognition (ICPR)*, pages 8376–8383. IEEE, 2021. 3, 7, 19
- [24] Kenta Oono and Taiji Suzuki. Graph neural networks exponentially lose expressive power for node classification. In *International Conference on Learning Representations*, 2020. 3
- [25] Johannes Klicpera, Stefan Weißenberger, and Stephan Günnemann. Diffusion improves graph learning. In *Proceedings of the 33rd International Conference on Neural Information Processing Systems*, 2019. 3, 8
- [26] Peter W Battaglia, Jessica B Hamrick, Victor Bapst, Alvaro Sanchez-Gonzalez, Vinicius Zambaldi, Mateusz Malinowski, Andrea Tacchetti, David Raposo, Adam Santoro, Ryan Faulkner, et al. Relational inductive biases, deep learning, and graph networks. *arXiv preprint arXiv:1806.01261*, 2018. 3
- [27] Fabrizio Frasca, Emanuele Rossi, Davide Eynard, Benjamin Chamberlain, Michael Bronstein, and Federico Monti. Sign: Scalable inception graph neural networks. In *ICML 2020 Workshop on Graph Representation Learning and Beyond*, 2020. 3
- [28] Pál András Papp, Karolis Martinkus, Lukas Faber, and Roger Wattenhofer. Dropgnn: Random dropouts increase the expressiveness of graph neural networks. In *35th Conference on Neural Information Processing Systems (NeurIPS)*, 2021. 3
- [29] Yu Rong, Wenbing Huang, Tingyang Xu, and Junzhou Huang. Dropedge: Towards deep graph convolutional networks on node classification. In *International Conference on Learning Representations*, 2020. 3
- [30] Deli Chen, Yankai Lin, Wei Li, Peng Li, Jie Zhou, and Xu Sun. Measuring and relieving the over-smoothing problem for graph neural networks from the topological view. *Proceedings of the AAAI Conference on Artificial Intelligence*, 34(04):3438–3445, Apr. 2020. 3
- [31] Diego Mesquita, Amauri Souza, and Samuel Kaski. Rethinking pooling in graph neural networks. *Advances in Neural Information Processing Systems*, 33:2220–2231, 2020. 4
- [32] Zhitao Ying, Jiaxuan You, Christopher Morris, Xiang Ren, Will Hamilton, and Jure Leskovec. Hierarchical graph representation learning with differentiable pooling. *Advances in neural information processing systems*, 31, 2018. 4
- [33] Filippo Maria Bianchi, Daniele Grattarola, and Cesare Alippi. Spectral clustering with graph neural networks for graph pooling. In *Proceedings of the 37th international conference on Machine learning*, pages 2729–2738. ACM, 2020. 4
- [34] Cătălina Cangea, Petar Veličković, Nikola Jovanović, Thomas Kipf, and Pietro Liò. Towards sparse hierarchical graph classifiers. In *In NeurIPS Workshop on Relational Representation Learning (R2L)*, 2018. 4
- [35] Hongyang Gao and Shuiwang Ji. Graph u-nets. In *international conference on machine learning*, pages 2083–2092. PMLR, 2019. 4

-
- [36] Ekagra Ranjan, Soumya Sanyal, and Partha Talukdar. Asap: Adaptive structure aware pooling for learning hierarchical graph representations. In *Proceedings of the AAAI Conference on Artificial Intelligence*, volume 34, pages 5470–5477, 2020. 4
 - [37] Jinheon Baek, Minki Kang, and Sung Ju Hwang. Accurate learning of graph representations with graph multiset pooling. In *International Conference on Learning Representations*, 2021. 4
 - [38] F. R. K. Chung. *Spectral Graph Theory*. American Mathematical Society, 1997. 4
 - [39] Ulrike von Luxburg, Agnes Radl, and Matthias Hein. Hitting and commute times in large random neighborhood graphs. *Journal of Machine Learning Research*, 15(52):1751–1798, 2014. 4
 - [40] Emmanuel Abbe. Community detection and stochastic block models: Recent developments. *J. Mach. Learn. Res.*, 18(1):6446–6531, jan 2017. 4, 7
 - [41] Morteza Alamgir and Ulrike von Luxburg. Phase transition in the family of p-resistances. In *Proceedings of the 24th International Conference on Neural Information Processing Systems*, NIPS’11, page 379–387, Red Hook, NY, USA, 2011. Curran Associates Inc. 5
 - [42] Thomas Bühler and Matthias Hein. Spectral clustering based on the graph p-laplacian. In *Proceedings of the 26th Annual International Conference on Machine Learning*, ICML ’09, page 81–88, New York, NY, USA, 2009. Association for Computing Machinery. 5, 7
 - [43] Pan Li and Olgica Milenkovic. Submodular hypergraphs: p-laplacians, Cheeger inequalities and spectral clustering. In Jennifer Dy and Andreas Krause, editors, *Proceedings of the 35th International Conference on Machine Learning*, volume 80 of *Proceedings of Machine Learning Research*, pages 3014–3023. PMLR, 10–15 Jul 2018. 5
 - [44] Gregory Berkolaiko, James B Kennedy, Pavel Kurasov, and Delio Mugnolo. Edge connectivity and the spectral gap of combinatorial and quantum graphs. *Journal of Physics A: Mathematical and Theoretical*, 50(36):365201, aug 2017. 5
 - [45] Zoran Stanić. Graphs with small spectral gap. *Electronic Journal of Linear Algebra*, 26:28, 2013. 5
 - [46] Daniel A. Spielman and Nikhil Srivastava. Graph sparsification by effective resistances. *SIAM Journal on Computing*, 40(6):1913–1926, 2011. 5
 - [47] D. J. Klein and M. Randić. Resistance distance. *Journal of Mathematical Chemistry*, 12(1):81–95, 1993. 5
 - [48] Huaijun Qiu and Edwin R. Hancock. Clustering and embedding using commute times. *IEEE Transactions on Pattern Analysis and Machine Intelligence*, 29(11):1873–1890, 2007. 5, 6
 - [49] Vedat Levi Alev, Nima Anari, Lap Chi Lau, and Shayan Oveis Gharan. Graph Clustering using Effective Resistance. In Anna R. Karlin, editor, *9th Innovations in Theoretical Computer Science Conference (ITCS 2018)*, volume 94 of *Leibniz International Proceedings in Informatics (LIPIcs)*, pages 41:1–41:16, Dagstuhl, Germany, 2018. Schloss Dagstuhl–Leibniz-Zentrum fuer Informatik. 6, 16
 - [50] Jian Kang and Hanghang Tong. N2n: Network derivative mining. In *Proceedings of the 28th ACM International Conference on Information and Knowledge Management*, CIKM ’19, page 861–870, New York, NY, USA, 2019. Association for Computing Machinery. 7, 18
 - [51] Joshua Batson, Daniel A. Spielman, Nikhil Srivastava, and Shang-Hua Teng. Spectral sparsification of graphs: Theory and algorithms. *Commun. ACM*, 56(8):87–94, aug 2013. 15

A Appendix

In Appendices A and B, we include a Table with the notation used in the paper and we provide an analysis of the diffusion and its relationship with curvature. Appendix C reports statistics and characteristics of the datasets used in the experimental section, describes additional experimental results and provides a summary of the computing infrastructure used in our experiments.

Table 2: Notation.

Symbol	Description
$G = (V, E)$	Graph = (Nodes, Edges)
\mathbf{A}	Adjacency matrix: $\mathbf{A} \in \mathbb{R}^{n \times n}$
\mathbf{X}	Feature matrix: $\mathbf{X} \in \mathbb{R}^{n \times F}$
v	Node $v \in V$ or $u \in V$
e	Edge $e \in E$
x	Features of node v : $x \in X$
n	Number of nodes: $n = V $
F	Number of features
\mathbf{D}	Degree diagonal matrix where d_v in D_{vv}
d_v	Degree of node v
$vol(G)$	Sum of the degrees of the graph $vol(G) = Tr[D]$
\mathbf{L}	Laplacian: $\mathbf{L} = \mathbf{D} - \mathbf{A}$
\mathbf{B}	Signed edge-vertex incidence matrix
\mathbf{b}_e	Incidence vector: Row vector of \mathbf{B} , with $\mathbf{b}_{e=(u,v)} = (\mathbf{e}_u - \mathbf{e}_v)$
\mathbf{v}_e	Projected incidence vector: $\mathbf{v}_e = \mathbf{L}^{+1/2}\mathbf{b}_e$
Γ	Ratio $\Gamma = \frac{1+\epsilon}{1-\epsilon}$
\mathcal{E}	Dirichlet Energy wrt \mathbf{L} : $\mathcal{E}(\mathbf{x}) := \mathbf{x}^T \mathbf{L} \mathbf{x}$
\mathcal{L}	Normalized Laplacian: $\mathcal{L} = \mathbf{I} - \mathbf{D}^{-1/2} \mathbf{A} \mathbf{D}^{-1/2}$
Λ	Eigenvalue matrix of \mathbf{L}
Λ'	Eigenvalue matrix of \mathcal{L}
λ_i	i -th eigenvalue of \mathbf{L}
λ_2	Second eigenvalue of \mathbf{L} : Spectral gap
λ'_i	i -th eigenvalue of \mathcal{L}
λ'_2	Second eigenvalue of \mathcal{L} : Spectral gap
\mathbf{F}	Matrix of eigenvectors of \mathbf{L}
\mathbf{G}	Matrix of eigenvectors of \mathcal{L}
\mathbf{f}_i	i eigenvector of \mathbf{L}
\mathbf{f}_2	Second eigenvector of \mathbf{L} : Fiedler vector
\mathbf{g}_i	i eigenvector of \mathcal{L}
\mathbf{g}_2	Second eigenvector of \mathcal{L} : Fiedler vector
$\tilde{\mathbf{A}}$	New Adjacency matrix
E'	New edges
H_{uv}	Hitting time between u and v
CT_{uv}	Commute time: $CT_{uv} = H_{uv} + H_{vu}$
R_{uv}	Effective resistance: $R_{uv} = CT_{uv}/vol(G)$
\mathbf{Z}	Matrix of commute times embeddings for all nodes in G
\mathbf{z}_u	Commute time embedding of node u
\mathbf{T}^{CT}	Resistance diffusion
\mathbf{S}	Cluster assignment matrix: $\mathbf{S} \in \mathbb{R}^{n \times 2}$
\mathbf{T}^{GAP}	GAP diffusion
\mathbf{e}_u	Unit vector with unit value at u and 0 elsewhere
$\nabla_{\tilde{\mathbf{A}}} \lambda_2$	Gradient of λ_2 wrt $\tilde{\mathbf{A}}$
$[\nabla_{\tilde{\mathbf{A}}} \lambda_2]_{ij}$	Gradient of λ_2 wrt $\tilde{\mathbf{A}}_{uv}$
p_u	Node curvature: $p_u := 1 - \frac{1}{2} \sum_{u \sim w} R_{uw}$
κ_{uv}	Edge curvature: $\kappa_{uv} := 2(p_u + p_v)/R_{uv}$

A.1 Appendix A

A.1.1 Notation

The Table 2 summarizes the notation used in the paper.

A.1.2 Analysis of \mathbf{T}^{CT}

First, we provide an answer to the following question:

Is resistance diffusion via \mathbf{T}^{CT} a principled way of preserving the Cheeger constant?

We answer the question above by linking Theorems 1 and 2 in the paper with the Lovász bound. The outline of our explanation follows three steps.

- **Proposition 1:** Theorem 1 (**Sparsification**) provides a principled way to bias the adjacency matrix so that the edges with the largest weights in the rewired graph correspond to the edges in graph's bottleneck.
- **Proposition 2:** Theorem 2 (**Cheeger vs Resistance**) can be used to show that increasing the effective resistance leads to a mild reduction of the Cheeger constant.
- **Proposition 3:** (Conclusion) The effectiveness of the above theorems to contain the Cheeger constant is constrained by the Lovász bound.

Next, we provide a thorough explanation of each of the propositions above.

Proposition 1 (Biasing). *Let $G' = \text{Sparsify}(G, q)$ be a sampling algorithm of graph $G = (V, E)$, where edges $e \in E$ are sampled with probability $q \propto R_e$ (proportional to the effective resistance). This choice is necessary to retain the global structure of G , i.e., to satisfy*

$$\forall \mathbf{x} \in \mathbb{R}^n : (1 - \epsilon) \mathbf{x}^T \mathbf{L}_G \mathbf{x} \leq \mathbf{x}^T \mathbf{L}_{G'} \mathbf{x} \leq (1 + \epsilon) \mathbf{x}^T \mathbf{L}_G \mathbf{x}, \quad (10)$$

with probability at least $1/2$ by sampling $O(n \log n / \epsilon^2)$ edges, with $1/\sqrt{n} < \epsilon \leq 1$, instead of $O(m)$, where $m = |E|$. In addition, this choice biases the uniform distribution in favor of critical edges in the graph.

Proof. We start by expressing the Laplacian \mathbf{L} in terms of the edge-vertex incidence matrix $\mathbf{B}_{m \times e}$:

$$\mathbf{B}_{eu} = \begin{cases} 1 & \text{if } u \text{ is the head of } e \\ -1 & \text{if } u \text{ is the tail of } e \\ 0 & \text{otherwise.} \end{cases} \quad (11)$$

where edges in undirected graphs are counted once, i.e. $e = (u, v) = (v, u)$. Then, we have $\mathbf{L} = \mathbf{B}^T \mathbf{B} = \sum_e \mathbf{b}_e \mathbf{b}_e^T$, where \mathbf{b}_e is a row vector (*incidence vector*) of \mathbf{B} , with $\mathbf{b}_{e=(u,v)} = (\mathbf{e}_u - \mathbf{e}_v)$. In addition, the Dirichlet energies can be expressed as norms:

$$\mathcal{E}(\mathbf{x}) = \mathbf{x}^T \mathbf{L} \mathbf{x} = \mathbf{x}^T \mathbf{B}^T \mathbf{B} \mathbf{x} = \|\mathbf{B} \mathbf{x}\|_2^2 = \sum_{e=(u,v) \in E} (\mathbf{x}_u - \mathbf{x}_v)^2. \quad (12)$$

As a result, the effective resistance R_e between the two nodes of an edge $e = (u, v)$ can be defined as

$$R_e = (\mathbf{e}_u - \mathbf{e}_v)^T \mathbf{L}^+ (\mathbf{e}_u - \mathbf{e}_v) = \mathbf{b}_e^T \mathbf{L}^+ \mathbf{b}_e \quad (13)$$

Next, we reformulate the spectral constraints in Eq. 10, i.e. $(1 - \epsilon) \mathbf{L}_G \preccurlyeq \mathbf{L}_{G'} \preccurlyeq (1 + \epsilon) \mathbf{L}_G$ as

$$\mathbf{L}_G \preccurlyeq \mathbf{L}_{G'} \preccurlyeq \Gamma \mathbf{L}_G, \quad \Gamma = \frac{1 + \epsilon}{1 - \epsilon}. \quad (14)$$

This simplifies the analysis, since the above expression can be interpreted as follows: the Dirichlet energies of $\mathbf{L}_{G'}$ are lower-bounded by those of \mathbf{L}_G and upper-bounded by Γ times the energies of \mathbf{L}_G . Considering that the energies define hyper-ellipsoids, the hyper-ellipsoid associated with $\mathbf{L}_{G'}$ is between the hyper-ellipsoids of \mathbf{L}_G and Γ times the \mathbf{L}_G .

The hyper-ellipsoid analogy provides a framework to proof that the inclusion relationships are preserved under scaling: $M\mathbf{L}_G M \preccurlyeq M\mathbf{L}_{G'} M \preccurlyeq M\Gamma\mathbf{L}_G M$ where M can be a matrix. In this case, if we set $M := (\mathbf{L}_G^+)^{1/2} = \mathbf{L}_G^{+1/2}$ we have:

$$\mathbf{L}_G^{+1/2} \mathbf{L}_G \mathbf{L}_G^{+1/2} \preccurlyeq \mathbf{L}_G^{+1/2} \mathbf{L}_{G'} \mathbf{L}_G^{+1/2} \preccurlyeq \mathbf{L}_G^{+1/2} \Gamma \mathbf{L}_G^{+1/2}, \quad (15)$$

which leads to

$$\mathbf{I}_n \preccurlyeq \mathbf{L}_G^{+1/2} \mathbf{L}_G \mathbf{L}_G^{+1/2} \preccurlyeq \Gamma \mathbf{I}_n. \quad (16)$$

We seek a Laplacian $\mathbf{L}_{G'}$ satisfying the *similarity constraints* in Eq. 14. Since $E' \subset E$, i.e. we want to remove structurally irrelevant edges, we can design $\mathbf{L}_{G'}$ in terms of considering *all* the edges E :

$$\mathbf{L}_{G'} := \mathbf{B}_G^T \mathbf{B}_G = \sum_e s_e \mathbf{b}_e \mathbf{b}_e^T \quad (17)$$

and let the similarity constraint define the sampling weights and the choice of e (setting $s_e \geq 0$ properly). More precisely:

$$\mathbf{I}_n \preccurlyeq \mathbf{L}_G^{+1/2} \sum_e \mathbf{b}_e \mathbf{b}_e^T \mathbf{L}_G^{+1/2} \preccurlyeq \Gamma \mathbf{I}_n. \quad (18)$$

Then if we define $\mathbf{v}_e := \mathbf{L}_G^{+1/2} \mathbf{b}_e$ as the *projected incidence vector*, we have

$$\mathbf{I}_n \preccurlyeq \sum_e s_e \mathbf{v}_e \mathbf{v}_e^T \preccurlyeq \Gamma \mathbf{I}_n. \quad (19)$$

Consequently, a spectral sparsifier must find $s_e \geq 0$ so that the above similarity constraint is satisfied. Since there are m edges in E , s_e must be zero for most of the edges. But, what are the best candidates to retain? Interestingly, the similarity constraint provides the answer. From Eq. 13 we have

$$\mathbf{v}_e^T \mathbf{v}_e = \|\mathbf{v}_e\|^2 = \|\mathbf{L}_G^{+1/2} \mathbf{b}_e\|_2^2 = \mathbf{b}_e^T \mathbf{L}_G^+ \mathbf{b}_e = R_e. \quad (20)$$

This result explains why sampling the edges with probability $q \propto R_e$ leads to a ranking of m edges of $G = (V, E)$ such that edges with large $R_e = \|\mathbf{v}_e\|^2$ are preferred⁶.

Algorithm 1 implements a deterministic greedy version of $\text{Sparsify}(G, q)$, where we build incrementally $E' \subset E$ by creating a budget of decreasing resistances $R_{e_1} \geq R_{e_2} \geq \dots \geq R_{e_{O(n \log n / \epsilon^2)}}.$ \square

Note that this rewiring strategy preserves the spectral similarities of the graphs, i.e. the global structure of $G = (V, E)$ is captured by $G' = (V, E')$.

Moreover, the maximum R_e in each graph determines an upper bound on the Cheeger constant and hence an upper bound on the size of the graph's bottleneck, as per the following proposition.

Proposition 2 (Resistance Diameter). *Let $G' = \text{Sparsify}(G, q)$ be a sampling algorithm of graph $G = (V, E)$, where edges $e \in E$ are sampled with probability $q \propto R_e$ (proportional to the effective resistance). Consider the resistance diameter $\mathcal{R}_{diam} := \max_{u,v} R_{uv}$. Then, for the pair of (u, v) does exist an edge $e = (u, v) \in E'$ in $G' = (V, E')$ such that $R_e = \mathcal{R}_{diam}$. As a result the Cheeger constant of G h_G is upper-bounded as follows:*

$$h_G \leq \frac{\alpha^\epsilon}{\sqrt{\mathcal{R}_{diam}} \cdot \epsilon} \text{vol}(S)^{\epsilon-1/2}, \quad (21)$$

with $0 < \epsilon < 1/2$ and $d_u \geq 1/\alpha$ for all $u \in V$.

⁶Although some of the elements of this section are derived from [51], we note that the Nikhil Srivastava's lectures at The Simons Institute (2014) are by far more clarifying.

Algorithm 1: GREEDYSparsify

Input : $G = (V, E), \epsilon \in (1/\sqrt{n}, 1], n = |V|$.

Output : $G' = (V, E')$ with $E' \subset E$ such that $|E'| = O(n \log n / \epsilon^2)$.

```

 $L \leftarrow \text{List}(\{\mathbf{v}_e : e \in E\})$ 
 $Q \leftarrow \text{Sort}(L, \text{descending, criterion}=\|\mathbf{v}_e\|^2)$        $\triangleright$  Sort candidate edges by descending Resistance
 $E' \leftarrow \emptyset$ 
 $\mathcal{I} \leftarrow \mathbf{0}_{n \times n}$ 
repeat
     $\mathbf{v}_e \leftarrow \text{pop}(Q)$                                  $\triangleright$  Remove the head of the queue
     $\mathcal{I} \leftarrow \mathcal{I} + \mathbf{v}_e \mathbf{v}_e^T$ 
    if  $\mathcal{I} \preccurlyeq \Gamma \mathbf{I}_n$  then
         $|E' \leftarrow E' \cup \{e\}$                                  $\triangleright$  Update the current budget of edges
    else
        return  $G' = (V, E')$ 
until  $Q = \emptyset$ 

```

Proof. The fact that the maximum resistance \mathcal{R}_{diam} is located in an edge is derived from two observations: a) Resistance is upper bounded by the shortest-path distance; and b) edges with maximal resistance are prioritized in (Proposition 1).

Theorem 2 states that any attempt to increase the graph's bottleneck in a multiplicative way (i.e. multiplying it by a constant $c \geq 0$) results in decreasing the effective resistances as follows:

$$R_{uv} \leq \left(\frac{1}{d_u^{2\epsilon}} + \frac{1}{d_v^{2\epsilon}} \right) \cdot \frac{1}{\epsilon \cdot c^2} \quad (22)$$

with $\epsilon \in [0, 1/2]$. This equation is called the *resistance bound*. Therefore, a multiplicative increase of the bottleneck leads to a quadratic decrease of the resistances.

Following Corollary 2 of [49], we obtain an upper bound of any h_S , i.e. the Cheeger constant for $S \subseteq V$ with $\text{vol}(S) \leq \text{vol}(G)/2$ – by defining c properly. In particular we are seeking a value of c that would lead to a contradiction, which is obtained by setting

$$c = \sqrt{\frac{\left(\frac{1}{d_{u^*}^{2\epsilon}} + \frac{1}{d_{v^*}^{2\epsilon}} \right)}{\mathcal{R}_{diam} \cdot \epsilon}}, \quad (23)$$

where (u^*, v^*) is a pair of nodes with maximal resistance, i.e. $R_{u^*v^*} = \mathcal{R}_{diam}$.

Consider now any other pair of nodes (s, t) with $R_{st} < \mathcal{R}_{diam}$. Following Theorem 2, if the bottleneck of h_S is multiplied by c , we should have

$$R_{st} \leq \left(\frac{1}{d_s^{2\epsilon}} + \frac{1}{d_t^{2\epsilon}} \right) \cdot \frac{1}{\epsilon \cdot c^2} = \left(\frac{1}{d_s^{2\epsilon}} + \frac{1}{d_s^{2\epsilon}} \right) \cdot \frac{\mathcal{R}_{diam}}{\left(\frac{1}{d_{u^*}^{2\epsilon}} + \frac{1}{d_{v^*}^{2\epsilon}} \right)}. \quad (24)$$

However, since $\mathcal{R}_{diam} \leq \left(\frac{1}{d_{u^*}^{2\epsilon}} + \frac{1}{d_{v^*}^{2\epsilon}} \right)$ we have that R_{st} can satisfy

$$R_{st} > \left(\frac{1}{d_s^{2\epsilon}} + \frac{1}{d_s^{2\epsilon}} \right) \cdot \frac{1}{\epsilon \cdot c^2} \quad (25)$$

which is a contradiction and enables

$$h_S \leq \frac{c}{\text{vol}(S)^{1/2-\epsilon}} \iff |\partial S| \leq c \cdot \text{vol}(S)^{1/2-\epsilon}. \quad (26)$$

Using c as defined in Eq. 23 and $d_u \geq 1/\alpha$ we obtain

$$c = \sqrt{\frac{\left(\frac{1}{d_u^{2\epsilon}} + \frac{1}{d_v^{2\epsilon}}\right)}{\mathcal{R}_{diam} \cdot \epsilon}} \leq \sqrt{\frac{\alpha^\epsilon}{\mathcal{R}_{diam} \cdot \epsilon}} \leq \frac{\alpha^\epsilon}{\sqrt{\mathcal{R}_{diam} \cdot \epsilon}}. \quad (27)$$

Therefore,

$$h_S \leq \frac{c}{vol(S)^{1/2-\epsilon}} \leq \frac{\frac{\alpha^\epsilon}{\sqrt{\mathcal{R}_{diam} \cdot \epsilon}}}{vol(S)^{1/2-\epsilon}} = \frac{\alpha^\epsilon}{\sqrt{\mathcal{R}_{diam} \cdot \epsilon}} \cdot vol(S)^{\epsilon-1/2}. \quad (28)$$

As a result, the Cheeger constant of $G = (V, E)$ is mildly reduced (by the square root of the maximal resistance). \square

Proposition 3 (Conclusion). *Let (u^*, v^*) be a pair of nodes (may be not unique) in $G = (V, E)$ with maximal resistance, i.e. $R_{u^*v^*} = \mathcal{R}_{diam}$. Then, the Cheeger constant h_G relies on the ratio between the maximal resistance \mathcal{R}_{diam} and its uninformative approximation $\left(\frac{1}{d_u^*} + \frac{1}{d_v^*}\right)$. The closer this ratio is to the unit, the easier it is to contain the Cheeger constant.*

Proof. The referred ratio above is the ratio leading to a proper c in Proposition 2. This is consistent with a Lovász regime where the spectral gap λ_2' has a moderate value. However, for regimes with very small spectral graphs, i.e. $\lambda_2' \rightarrow 0$, according to the Lovász bound, $\mathcal{R}_{diam} \gg \left(\frac{1}{d_u^*} + \frac{1}{d_v^*}\right)$ and hence the Cheeger constant provided by Proposition 2 will tend to zero. \square

We conclude that we can always find a moderate upper bound for the Cheeger constant of $G = (V, E)$, provided that the regime of the Lovász bound is also moderate. Therefore, as the global properties of $G = (V, E)$ are captured by $G' = (V, E')$, a moderate Cheeger constant, when achievable, also controls the bottlenecks in $G' = (V, E')$.

Our methodology has focused on first exploring the properties of the commute times / effective resistances in $G = (V, E)$. Next, we have leveraged the spectral similarity to reason about the properties –particularly the Cheeger constant– of $G = (V, E')$. In sum, we conclude that resistance diffusion via \mathbf{T}^{CT} is a principled way of preserving the Cheeger constant of $G = (V, E)$.

A.1.3 Resistance-based Curvatures

We refer to recent work by Devriendt and Lambiotte [22] to complement the contributions of Topping et al. [21] regarding the use of curvature to rewire the edges in a graph. The new definition of curvature given in [21] is related to the resistance distance and thus it is learnable with the proposed framework (CT-LAYER). Actually, the Balanced-Forman curvature (Definition 1 in [21]) relies on the uninformative approximation of the resistance distance.

Figure 3 illustrates the relationship between effective resistances / commute times and curvature on an exemplary graph from the COLLAB dataset.

As seen in the Figure, effective resistances prioritize the edges connecting outer nodes with hubs or central nodes, while the intra-community connections are de-prioritized. This observation is consistent with the aforementioned theoretical explanations about preserving the bottleneck while breaking the intra-cluster structure. In addition, we also observe that the original edges between hubs have been deleted or have been extremely down-weighted.

Regarding curvature, hubs or central nodes have the lowest node curvature (this curvature increases with the number of nodes in a cluster/community). Edge curvatures, which rely on node curvatures, depend on the long-term neighborhoods of the connecting nodes. In general, edge curvatures can be seen as a smoothed version –since they integrate node curvatures– of the inverse of the resistance distances.

We observe that edges linking nodes of a given community with hubs tend to have similar edge-curvature values. However, edges linking nodes of different communities with hubs have different edge curvatures

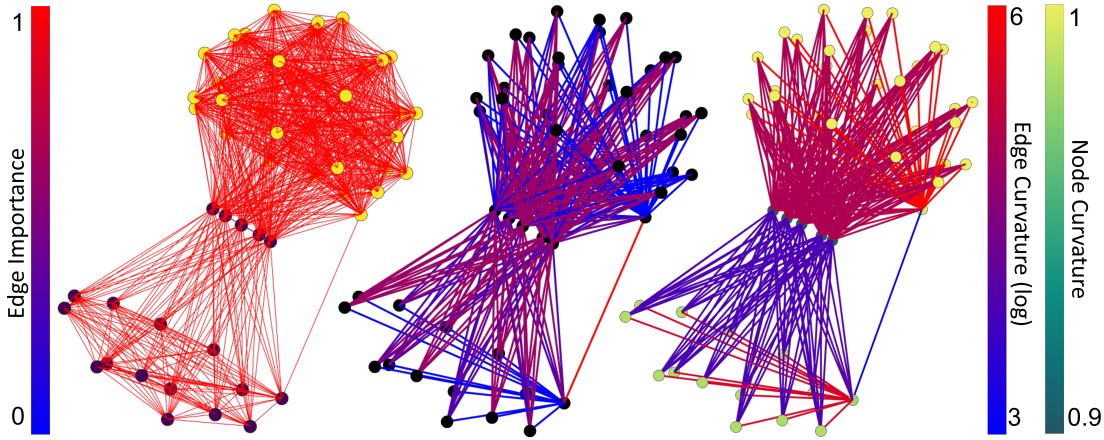


Figure 3: Left: Original graph with nodes colored as Louvain communities. Middle: \mathbf{T}^{CT} learnt by CT-LAYER with edges colors as node importance $[0,1]$. Right: Node and edge curvature: \mathbf{T}^{CT} using $p_u := 1 - \frac{1}{2} \sum_{w \sim u} \mathbf{T}_{uw}^{CT}$ and $\kappa_{uv} := 2(p_u + p_v)/\mathbf{T}_{uv}^{CT}$ with edge and node curvatures as color.

(Figure 3-right). This is due to the different number of nodes belonging to each community, and to their different average degree inside their respective communities (property 1 of Theorem 3).

Finally, note that the range of edge curvatures is larger than that of resistance distances. The sparsifier transforms a uniform distribution of the edge weights into a less entropic one: in the example of Figure 3 we observe a power-law distribution of edge resistances. As a result, $\kappa_{uv} := 2(p_u + p_v)/\mathbf{T}_{uv}^{CT}$ becomes very large on average (edges with infinite curvature are not shown in the plot) and a log scale is needed to appreciate the differences between edge resistances and edge curvatures.

A.2 Appendix B

A.2.1 Spectral Gradients

The proposed GAP-LAYER relies on gradients wrt the Laplacian eigenvalues, and particularly the spectral gap (λ_2 for \mathbf{L} and λ'_2 wrt \mathcal{L}). Although the GAP-LAYER inductively rewrites the adjacency matrix \mathbf{A} so that λ_2 is minimized, the gradients derived in this section may also be applied for gap maximization.

Note that while our cost function $L_{Fiedler} = \|\tilde{\mathbf{A}} - \mathbf{A}\|_F + \alpha(\lambda_2^*)^2$, with $\lambda_2^* \in \{\lambda_2, \lambda'_2\}$, relies on an eigenvalue, we *do not compute it explicitly*, as its computation has a complexity of $O(n^3)$ and would need to be computed in every learning iteration. Instead, we learn an approximation of λ_2 's eigenvector \mathbf{f}_2 and use its Dirichlet energy $\mathcal{E}(\mathbf{f}_2)$ to approximate the eigenvalue. In addition, since $\mathbf{g}_2 = \mathbf{D}^{1/2}\mathbf{f}_2$, we first approximate \mathbf{g}_2 and then approximate λ'_2 from $\mathcal{E}(\mathbf{g}_2)$.

Gradients of the Ratio-cut Approximation. Let \mathbf{A} be the adjacency matrix of $G = (V, E)$; and $\tilde{\mathbf{A}}$, a matrix similar to the original adjacency but with minimal λ_2 . Then, the gradient of λ_2 wrt each component of $\tilde{\mathbf{A}}$ is given by

$$\nabla_{\tilde{\mathbf{A}}} \lambda_2 := \text{Tr} \left[(\nabla_{\tilde{\mathbf{L}}} \lambda_2)^T \cdot \nabla_{\tilde{\mathbf{A}}} \tilde{\mathbf{L}} \right] = \text{diag}(\mathbf{f}_2 \mathbf{f}_2^T) \mathbf{1} \mathbf{1}^T - \mathbf{f}_2 \mathbf{f}_2^T, \quad (29)$$

where $\mathbf{1}$ is the vector of n ones; and $[\nabla_{\tilde{\mathbf{A}}} \lambda_2]_{ij}$ is the gradient of λ_2 wrt $\tilde{\mathbf{A}}_{uv}$. The above formula is an instance of the network derivative mining approach [50]. In this framework, λ_2 is seen as a function of $\tilde{\mathbf{A}}$ and $\nabla_{\tilde{\mathbf{A}}} \lambda_2$, the gradient of λ_2 wrt $\tilde{\mathbf{A}}$, comes from the chain rule of the matrix derivative $\text{Tr} \left[(\nabla_{\tilde{\mathbf{L}}} \lambda_2)^T \cdot \nabla_{\tilde{\mathbf{A}}} \tilde{\mathbf{L}} \right]$.

More precisely,

$$\nabla_{\tilde{\mathbf{L}}} \lambda_2 := \frac{\partial \lambda_2}{\partial \tilde{\mathbf{L}}} = \mathbf{f}_2 \mathbf{f}_2^T, \quad (30)$$

is a matrix relying on an outer product (correlation). In the proposed GAP-LAYER, since \mathbf{f}_2 is approximated by:

$$\mathbf{f}_2(u) = \begin{cases} +1/\sqrt{n} & \text{if } u \text{ belongs to the first cluster} \\ -1/\sqrt{n} & \text{if } u \text{ belongs to the second cluster} \end{cases}, \quad (31)$$

i.e. we discard the $O\left(\frac{\log n}{n}\right)$ from Eq. 31 (the non-linearities conjectured in [23]) in order to simplify the analysis. After reordering the entries of \mathbf{f}_2 for the sake of clarity, $\mathbf{f}_2 \mathbf{f}_2^T$ is the following block matrix:

$$\mathbf{f}_2 \mathbf{f}_2^T = \begin{bmatrix} 1/n & -1/n \\ -1/n & 1/n \end{bmatrix} \text{ whose diagonal matrix is } \text{diag}(\mathbf{f}_2 \mathbf{f}_2^T) = \begin{bmatrix} 1/n & 0 \\ 0 & 1/n \end{bmatrix} \quad (32)$$

Then, we have

$$\nabla_{\tilde{\mathbf{A}}} \lambda_2 = \begin{bmatrix} 1/n & 1/n \\ 1/n & 1/n \end{bmatrix} - \begin{bmatrix} 1/n & -1/n \\ -1/n & 1/n \end{bmatrix} = \begin{bmatrix} 0 & 2/n \\ 2/n & 0 \end{bmatrix} \quad (33)$$

which explains the results in Figure 1-left: edges linking nodes belonging to the same cluster remain unchanged whereas inter-cluster edges have a gradient of $2/n$. This provides a simple explanation for $\mathbf{T}^{GAP} = \tilde{\mathbf{A}}(\mathbf{S}) \odot \mathbf{A}$. The additional masking added by the adjacency matrix ensures that we do not create new links.

Gradients Normalized-cut Approximation. Similarly, using λ'_2 for graph rewiring leads to the following complex expression:

$$\begin{aligned} \nabla_{\tilde{\mathbf{A}}} \lambda'_2 &:= \text{Tr} \left[(\nabla_{\tilde{\mathcal{L}}} \lambda_2)^T \cdot \nabla_{\tilde{\mathbf{A}}} \tilde{\mathcal{L}} \right] = \\ &\mathbf{d}' \left\{ \mathbf{g}_2^T \tilde{\mathbf{A}}^T \tilde{\mathbf{D}}^{-1/2} \mathbf{g}_2 \right\} \mathbf{1}^T + \mathbf{d}' \left\{ \mathbf{g}_2^T \tilde{\mathbf{A}} \tilde{\mathbf{D}}^{-1/2} \mathbf{g}_2 \right\} \mathbf{1}^T + \tilde{\mathbf{D}}^{-1/2} \mathbf{g}_2 \mathbf{g}_2^T \tilde{\mathbf{D}}^{-1/2}. \end{aligned} \quad (34)$$

However, since $\mathbf{g}_2 = \mathbf{D}^{1/2} \mathbf{f}_2$ and $\mathbf{f}_2 = \mathbf{D}^{-1/2} \mathbf{g}_2$, the gradient may be simplified as follows:

$$\begin{aligned} \nabla_{\tilde{\mathbf{A}}} \lambda'_2 &:= \text{Tr} \left[(\nabla_{\tilde{\mathcal{L}}} \lambda_2)^T \cdot \nabla_{\tilde{\mathbf{A}}} \tilde{\mathcal{L}} \right] = \\ &\mathbf{d}' \left\{ \mathbf{f}_2^T \tilde{\mathbf{D}}^{1/2} \tilde{\mathbf{A}}^T \mathbf{f}_2 \right\} \mathbf{1}^T + \mathbf{d}' \left\{ \mathbf{f}_2^T \tilde{\mathbf{D}}^{1/2} \tilde{\mathbf{A}} \mathbf{f}_2 \right\} \mathbf{1}^T + \tilde{\mathbf{D}}^{-1/2} \mathbf{f}_2 \mathbf{f}_2^T \tilde{\mathbf{D}}^{-1/2}. \end{aligned} \quad (35)$$

In addition, considering symmetry for the undirected graph case, we obtain:

$$\nabla_{\tilde{\mathbf{A}}} \lambda'_2 := \text{Tr} \left[(\nabla_{\tilde{\mathcal{L}}} \lambda_2)^T \cdot \nabla_{\tilde{\mathbf{A}}} \tilde{\mathcal{L}} \right] = 2\mathbf{d}' \left\{ \mathbf{f}_2^T \tilde{\mathbf{D}}^{1/2} \tilde{\mathbf{A}} \mathbf{f}_2 \right\} \mathbf{1}^T + \tilde{\mathbf{D}}^{-1/2} \mathbf{f}_2 \mathbf{f}_2^T \tilde{\mathbf{D}}^{-1/2}.$$

where \mathbf{d}' is a $n \times 1$ negative vector including derivatives of degree wrt adjacency and related terms. The obtained gradient is composed of two terms.

The first term contains the matrix $\tilde{\mathbf{D}}^{1/2} \tilde{\mathbf{A}}$ which is the adjacency matrix weighted by the square root of the degree; $\mathbf{f}_2^T \tilde{\mathbf{D}}^{1/2} \tilde{\mathbf{A}} \mathbf{f}_2$ is a quadratic form (similar to a Dirichlet energy for the Laplacian) which approximates an eigenvalue of $\tilde{\mathbf{D}}^{1/2} \tilde{\mathbf{A}}$. We plan to further analyze the properties of this term in future work.

The second term, $\tilde{\mathbf{D}}^{-1/2} \mathbf{f}_2 \mathbf{f}_2^T \tilde{\mathbf{D}}^{-1/2}$, downweights the correlation term for the Ratio-cut case $\mathbf{f}_2 \mathbf{f}_2^T$ by the degrees as in the normalized Laplacian. This results in a normalization of the Fiedler vector: $-1/n$ becomes $-\sqrt{d_u d_v}/n$ at the uv entry and similarly for $1/n$, i.e. each entry contains the average degree assortativity.

A.3 Appendix C

In this section, we provide details about the graphs contained in each of the datasets used in our experiments and report additional experimental results.

A.3.1 Datasets statistics

Table 3 depicts the number of nodes, edges, average degree, assortativity, number of triangles, transitivity and clustering coefficients (mean and standard deviation) of all the graphs contained in each of the benchmark datasets used in our experiments. As seen in the Table, the datasets are very diverse in their characteristics.

Table 3: Dataset statistics.

	Nodes	Edges	AVG Degree	Triangles	Transitivity	Clustering
REDDIT-BINARY	429.6 ± 554	497.7 ± 622	2.33 ± 0.3	24 ± 41	0.01 ± 0.02	0.04 ± 0.06
IMDB-BINARY	19.7 ± 10	96.5 ± 105	8.88 ± 5.0	391 ± 868	0.77 ± 0.15	0.94 ± 0.03
COLLAB	74.5 ± 62	2457 ± 6438	37.36 ± 44	$12 \times 10^4 \pm 48 \times 10^4$	0.76 ± 0.21	0.89 ± 0.08
MUTAG	2.2 ± 0.1	19.8 ± 5.6	2.18 ± 0.1	0.00 ± 0.0	0.00 ± 0.00	0.00 ± 0.00
PROTEINS	39.1 ± 45.8	72.8 ± 84.6	3.73 ± 0.4	27.4 ± 30	0.48 ± 0.20	0.51 ± 0.23
CIFAR10	117.6 ± 4.2	469.1 ± 18.4	7.98 ± 0.1	502 ± 30	0.45 ± 0.01	0.45 ± 0.01
MNIST	70.6 ± 6.8	281.6 ± 27.8	7.98 ± 0.1	316 ± 33	0.47 ± 0.01	0.48 ± 0.01
ENZYMES	32.6 ± 15.3	62.1 ± 25.4	3.86 ± 0.5	25.5 ± 12	0.42 ± 0.17	0.45 ± 0.19

In addition, Figure 4 depicts the histograms of the average node degrees for all the graphs in each of the eight datasets used in our experiments. The datasets are also very diverse in terms of topology, corresponding to social networks, biochemical networks and meshes.

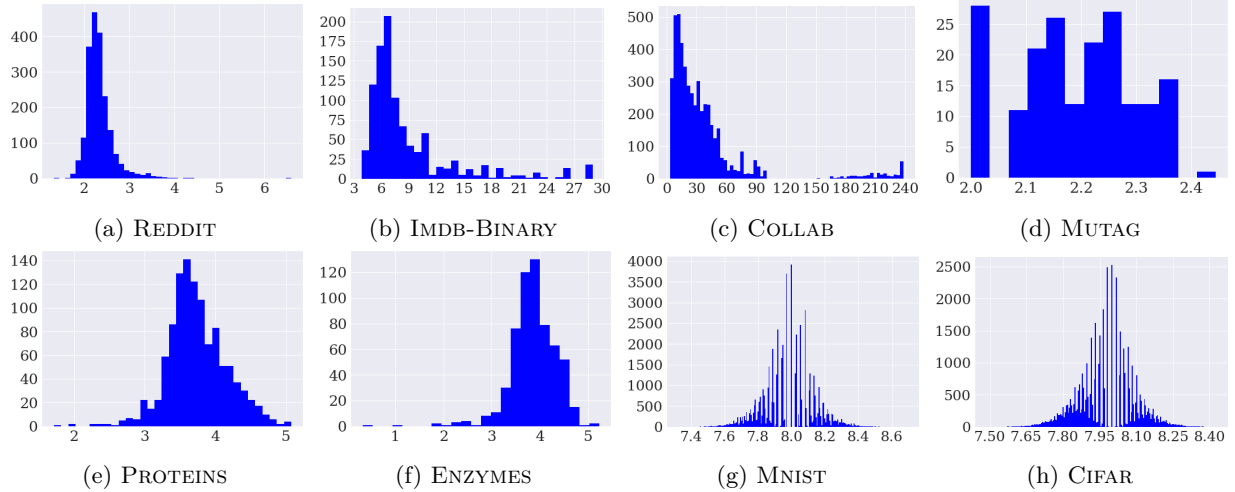


Figure 4: Degree histogram of the average degree of all the graphs in each of the datasets.

A.3.2 GNN architectures

Figure 5 shows the GNN architectures used in the experiments explained in section 4 in the manuscript. The calculation of \mathbf{T}^{GAP} and \mathbf{T}^{CT} are given in Theorems 2 and 1.

A.3.3 Additional Experiments

Although our method performs better in graphs where bottlenecks could exist (scale-free networks), we carry out additional experiments with two different kinds of graphs: planar and meshes. Results are shown in Table 4. We observe that neither CT-LAYER nor GAP-LAYER show improvements wrt the baseline architectures in planar (ENZYMES) and mesh (CIFAR10 and MNIST) graphs. Note that all the graphs in these datasets have node features.

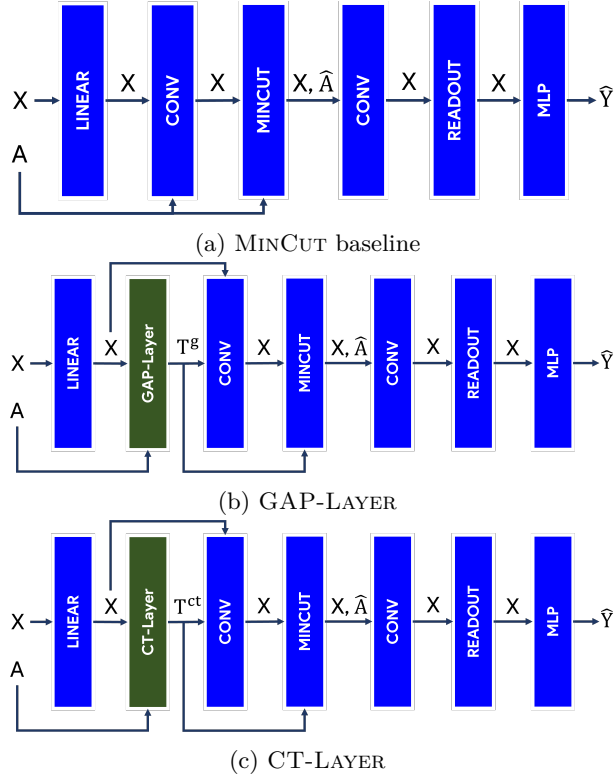


Figure 5: Diagrams of the GNNs used in the experiments.

Table 4: Experimental results on additional benchmark datasets with planar and mesh topologies.

	CIFAR10	MNIST	ENZYMES
MinCut (baseline)	30.13 ± 1.54	36.38 ± 2.48	31.50 ± 3.35
MinCut + DIGL	32.20 ± 1.48	33.30 ± 1.55	28.50 ± 3.32
CT-LAYER	<u>31.07 ± 0.17</u>	<u>35.01 ± 0.49</u>	32.50 ± 3.70
GAP-LAYER (Rcut)	26.12 ± 0.44	25.14 ± 0.42	30.75 ± 4.34
GAP-LAYER (Ncut)	26.34 ± 0.41	25.12 ± 0.39	29.42 ± 4.66

A.3.4 DiffWire: Combination of GAP-LAYER and CT-LAYER

A natural step in our proposed approach would be to combine CT-LAYER and GAP-LAYER in the same architecture, which we refer to as DIFFWIRE. The most immediate architecture combining the proposed layers would consist of concatenating them, such that the output of GAP-LAYER would be the input to CT-LAYER. However, preliminary experiments with such an architecture showed an adversarial behavior of both layers, leading to non-competitive results. We obtained the best experimental results with an architecture composed of 2 branches, one for each rewiring method, as shown in Figure 6.

Note that in the DIFFWIRE architecture, the MINCUT pooling layer clusters the features based on the original adjacency matrix \mathbf{A} instead of using \mathbf{T}^{GAP} or \mathbf{T}^{CT} as we assume that the previous rewiring layers have already controlled the over-smoothing problem with respect to the node features.

Table 5 summarizes the results of using DIFFWIRE for a graph classification task in the same benchmark datasets. For clarity, we also include the results obtained with CT-LAYER and GAP-LAYER in isolation. We observe that there is no clear benefit in combining the two layers in most of the datasets. However, DIFFWIRE outperforms the individual layers in two cases: the COLLAB dataset and datasets with mesh-graphs.

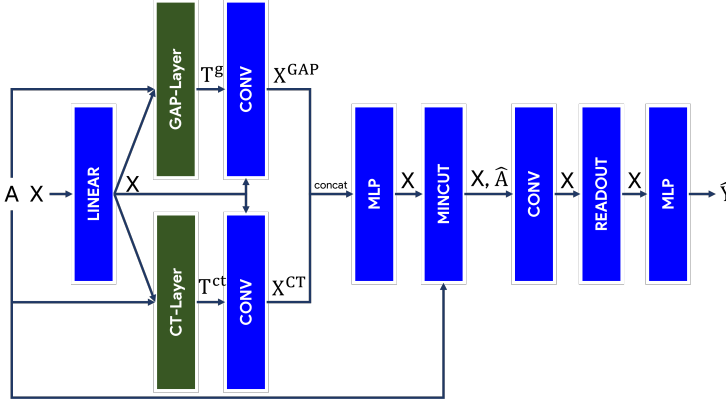


Figure 6: DIFFWIRE architecture: Using 2 branches for GAP-LAYER and CT-LAYER.

Table 5: Experimental results of the interplay between 2 layers in the DIFFWIRE architecture. Best result of each row is marked in bold and runner-up is underlined. Note that the results of CT-LAYER, GAP-LAYER (Rcut) and GAP-LAYER (Ncut) are repeated from Tables 1 and 4 in the paper.

	CT-LAYER	GAP-LAYER (Rcut)	GAP-LAYER (Ncut)	DIFFWIRE
REDDIT*	78.45 ± 4.59	<u>77.63 ± 4.96</u>	76.00 ± 5.30	77.17 ± 5.57
IMBD*	<u>69.84 ± 4.60</u>	69.93 ± 3.32	68.80 ± 3.10	69.80 ± 2.11
COLLAB*	<u>69.87 ± 2.40</u>	64.47 ± 4.07	65.89 ± 4.90	72.24 ± 2.13
MUTAG	86.05 ± 4.99	<u>86.90 ± 4.00</u>	<u>86.90 ± 4.00</u>	<u>86.90 ± 4.83</u>
PROTEINS	75.38 ± 2.97	75.03 ± 3.09	<u>75.34 ± 2.10</u>	74.91 ± 2.26
SBM*	81.40 ± 11.7	<u>90.80 ± 7.00</u>	92.26 ± 2.92	90.20 ± 4.51
ERDOS*	79.06 ± 9.89	79.26 ± 10.46	82.26 ± 3.2	<u>79.60 ± 4.39</u>
CIFAR	<u>31.07 ± 0.17</u>	26.12 ± 0.44	26.34 ± 0.41	41.19 ± 0.87
MNIST	<u>35.01 ± 0.49</u>	25.14 ± 0.42	25.12 ± 0.39	47.60 ± 1.40
ENZYMES	32.50 ± 3.70	30.75 ± 4.34	29.42 ± 4.66	<u>31.22 ± 3.70</u>

As per Table 3, COLLAB contains very dense graphs –with a high number of edges and triangles and a large clustering coefficient– where the combination of CT-LAYER and GAP-LAYER provides complementary representations. Regarding mesh graphs (e.g. CIFAR10 and MNIST), the parallel branches control the over-smoothing and the use of the original adjacency matrix in the MINCUT pooling layer ensures the preservation of the original topology.

A.3.5 Computing infrastructure

Table 6 summarizes the computing infrastructure used in our experiments.

Table 6: Computing infrastructure.

Component	Details
GPU	2x A100-SXM4-40GB
RAM	1 TiB
CPU	255x AMD 7742 64-Core @ 2.25 GHz
OS	Ubuntu 20.04.4 LTS